

ARTICLES

 $\pi^+ + d \rightarrow p + p$ below 21 MeV

B. G. Ritchie, T. D. Averett,* D. Rothenberger,[†] and J. R. Tinsley[‡]
Arizona State University, Tempe, Arizona 85287

R. C. Minehart, K. Giovanetti,[§] and L. C. Smith
University of Virginia, Charlottesville, Virginia 22903

G. S. Blanpied and B. M. Freedom
University of South Carolina, Columbia, South Carolina 29203
 (Received 31 July 1992)

Absolute total and differential cross sections for the reaction $\pi^+ + d \rightarrow p + p$ have been measured for pion energies from 3.7 to 20.5 MeV. A crossed-field velocity separator was used to enhance the purity of the pion beam, and a deuterated scintillator was used both as the target and to count the incident flux. The total cross sections are 4.0 ± 0.5 , 4.4 ± 0.2 , 4.2 ± 0.2 , 4.2 ± 0.2 , and 4.8 ± 0.3 mb for incident pion energies of 3.7, 5.0, 9.6, 15.2, and 20.5 MeV, respectively. The measured differential cross sections indicate the presence of p -wave strength at all energies studied and are in good agreement with recent measurements for the reaction $n + p \rightarrow d + \pi^0$ near threshold and a recent parametrization of the total and differential cross sections for the process.

PACS number(s): 25.80.Ls, 25.10.+s

I. INTRODUCTION

Studies of the reaction $\pi NN \rightarrow NN$ are of importance due to the fundamental role pion exchange plays in theoretical treatments of nuclear phenomena. The loosely bound deuteron provides an excellent laboratory for testing the microscopic understanding of this process. Theoretical attempts to explain the phenomena associated with this reaction have benefited during the past decade from numerous experiments which have provided precise data on various observables, particularly the total and differential cross sections for energies above 20 MeV. However, until recently the only published data for the $\pi^+ + d \rightarrow p + p$ reaction below 19 MeV were total cross sections measured by Rose [1]. These data possess large uncertainties, the smallest being approximately 8%. No differential cross sections have been published for this reaction below 19 MeV.

The main reason for the lack of data is that formation

of low energy pion beams with sufficient purity and intensity is experimentally difficult. Otherwise, the detection of the energetic protons emerging from the pion absorption reaction $\pi^+ + d \rightarrow p + p$ is straightforward. Measurement of the inverse pion production reaction is complicated by the difficulty in determining the scattering angles of the reaction products, whose energies are low and which are strongly boosted into the forward hemisphere, requiring large corrections for finite acceptance. The related reactions, $n + p \rightarrow d + \pi^0$ and its inverse, are complicated by the presence of neutral particles in both the entrance and exit channels.

Hutcheon *et al.* have recently published [2, 3] measurements of the total and differential cross sections for the reaction $n + p \rightarrow d + \pi^0$ near threshold. Using detailed balance and charge independence, their measurements can be related to measurements of $\pi^+ + d \rightarrow p + p$ with incident pion energies from less than 1 MeV to 7 MeV. The cross sections obtained in that work were normalized with respect to measurements for pp elastic scattering, and indicated the presence of p -wave contributions to the reaction amplitudes down to the lowest energies measured.

Recently, we published an overview [4] of new measurements of the total and differential cross sections for $\pi^+ + d \rightarrow p + p$ at energies below 21 MeV which overlap the energy range of the data of Ref. [5] and the data of Hutcheon *et al.* In this paper we give a more detailed description of the experimental techniques employed to make those measurements and tabulate the differential

*Present address: University of Virginia, Charlottesville, VA 22903.

[†]Present address: Naval Technical Information Center, Suitland, MD 20023.

[‡]Present address: EG&G, Santa Barbara, CA 93116.

[§]Present address: James Madison University, Harrisonburg, VA 22802.

cross sections determined for 3.7, 5.0, 9.6, 15.2, and 20.5 MeV.

II. EXPERIMENTAL PROCEDURE

The experiment was performed using the Low Energy Pion (LEP) Channel [6] at the Clinton P. Anderson Meson Physics Facility. The experimental apparatus used for all the measurements reported here is shown schematically in Fig. 1. In this section the apparatus and experimental techniques are described in detail.

A. Deuterated scintillator target

A square of deuterated polystyrene scintillator, Bicron BC-436, 2 cm on each side and 0.119 ± 0.001 cm thick, provided an active target. It was located 47.0 ± 0.5 cm downstream from the exit window of the drift tube following the quadrupole doublet, as shown in Fig. 1, and oriented perpendicular ($90^\circ \pm 2^\circ$) to the incident beam, as measured with an optical transit. The scintillator was wrapped with a single layer of 0.20 mm thick aluminum foil as an ambient light shield and scintillation light reflector and viewed by a standard 5 cm diameter photomultiplier tube and base to count the beam particles passing through the target.

The nominal deuteron/hydrogen ratio for the material had been determined to be 20.4 by the manufacturer prior to the experiment. After the experiment, the scintillator target material was independently assayed by infrared and nuclear magnetic resonance techniques. These assays yielded a deuteron areal density of 4.70×10^{21} deuterons/cm², with an uncertainty of 2.2%; this value was in agreement with specifications supplied by the manufacturer.

This deuterated scintillator target was also used to measure the beam flux on target, which was limited to 10^6 s to control pileup. As discussed below, the scintillator was essential in monitoring the composition of the LEP beam and determining incident pion flux.

B. Generation of pion beams

The LEP channel was operated in the standard manner to provide pion beams of 10.7, 16.0, and 21.2 MeV at the exit of the channel, with a channel momentum acceptance of 2.0, 1.0, and 2.5 %, respectively. As shown in Fig. 1, the pion beam then entered a crossed magnetic and electric field velocity separator which greatly improved the purity of the pion beam incident on the deuterated scintillator target.

The crossed-field separator design incorporated two stainless steel electrodes with parallel surfaces approximately 150 cm long in the direction of the undeflected particle trajectory and 20 cm high perpendicular to that trajectory. The electrodes and magnet coils for the separator were enclosed in an independent vacuum box approximately 0.53 m high, 0.53 m wide, and 1.90 m in length, maintained with a nominal operating pressure between 10^{-5} and 10^{-7} torr. The gap between the elec-

trodes was 10 cm. The separator was operated with an electric potential of 230 kV for the 10.7 MeV channel setting, and 300 kV for the other channel beam energies. The corresponding integrated magnetic field strengths $\int B \cdot dl$ at 10.7, 16.0, and 21.2 MeV were 27.7, 30.1, and 32.2 kG cm, respectively.

A quadrupole doublet was used after the velocity separator to focus the beam onto the target. An evacuated drift tube was attached to the doublet to minimize multiple scattering in air prior to the beam striking the target. The entire length of the separator, the quadrupole doublet, and the drift tube was 5.22 m.

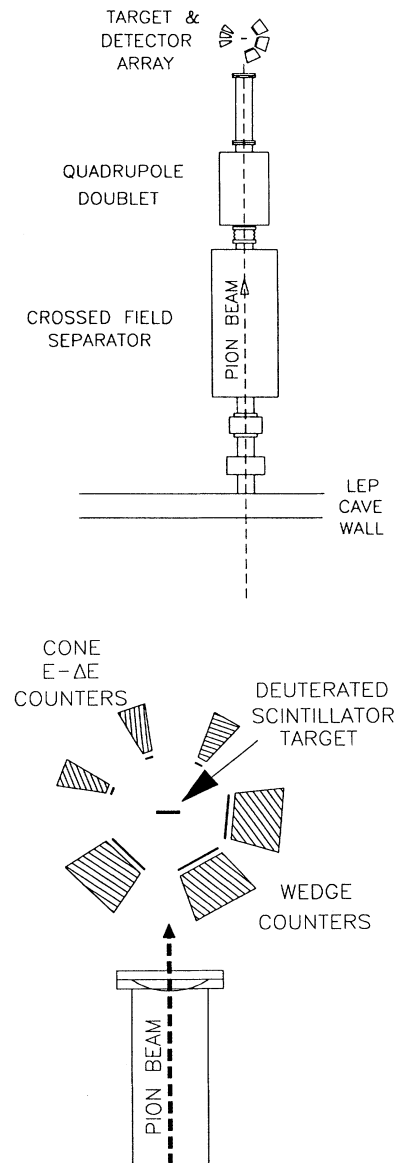


FIG. 1. Schematic layout of the apparatus used in this experiment. (a) The relative positions of the elements of the separator, associate quadrupoles, and the detector array as described in the text. (b) Additional details of the arrangement of the target and detection system.

The beam spot sizes were measured prior to data runs using a multiwire profile monitor at the target position with the target scintillator removed from the array. The same monitor was also used to tune and position the beam spot onto the target scintillator. With the separator off, the beam spots were measured to be approximately 1.0 cm FWHM vertically and 1.6 cm FWHM horizontally. With the separator on, the beam intensity was too low for the profile monitor to provide an accurate measurement of the spot sizes. However, photographic film exposed in the beam indicated that the separated beam spot was approximately the same size and shape as that obtained without the separator.

Monte Carlo simulations of the channel, velocity filter, quadrupole doublet, and detector array shown in Fig. 1 were used to calculate the energy distribution of the pions at the center of the scintillator target. The simulation included the effects of the vacuum window, the air drift space between the vacuum window and target, and the foil surrounding the target. The mean energies of the three beams determined from the results of the simulations, shown in Fig. 2, are 9.6, 15.2, and 20.5 MeV.

To achieve lower energies, graphite and aluminum degraders identical in area to the plastic scintillator target were placed in the 9.6 MeV beam directly against the upstream aluminum foil wrapping of the scintillator target. The thicknesses of the degraders were measured at nine places across the surface of each and found to be uniform with relative uncertainties of about 2%. Two combinations of degraders were used to obtain pion energies of 3.7 and 5.0 MeV at the center of the target. The results of simulations of the pion energy distributions at the center of the target for these lowest energy beams are also shown in Fig. 2.

C. Flux monitoring

Particle flux through the target scintillator was measured continuously during the data taking runs. The photomultiplier tube signal from the target scintillator was fed to a discriminator with a threshold setting well below the pulse height for minimum ionizing particles. Logic signals of 15, 40, 60, and 100 ns width from this target scintillator discriminator were counted by four separate scalars to provide dead-time corrections. With the exception of the 3.7 MeV data, these scalar values could be fit extremely well using only a linear time dependence. Extrapolation to “zero pulse width” using this linear fit yielded a dead-time corrected value for the number of target scintillator pulses for each run. Typical dead-time corrections were on the order of 3%, with relative uncertainties typically less than 10% of the correction. These dead-time uncertainties were negligible in comparison to the uncertainties in the pion fraction estimates described below.

At 3.7 MeV a significant fraction of the pions stopped in the target and subsequently decayed into muons. If the decay occurred after any of the scaler logic pulses noted above had returned to zero, a second count was generated in that scaler. The double counting is greatest

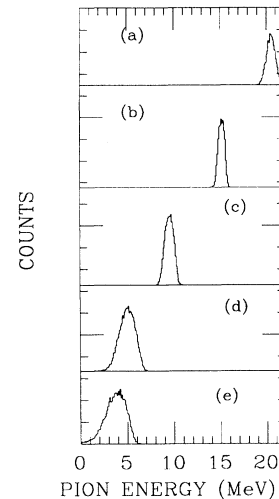


FIG. 2. Results of Monte Carlo simulations of the beam energy distributions at the center of the target, as described in the text. (a)–(e) Mean pion kinetic energies of 20.5, 15.2, 9.6, 5.0, and 3.7 MeV, respectively.

for the scaler with the smallest pulse width. The fraction of stopped pions giving double counts is $\exp(-t_w/\tau)$, where t_w is the width of the pulse and τ is the pion lifetime. To correct for the double counting, the counts from the four scalers were fit to the sum of a linear term and an exponential term. The linear term provided the dead-time estimates as noted above.

To check the validity of this fitting procedure, a fit to the 3.7 MeV scaler values was made treating the pion life time as a free parameter. The best fit was obtained using the accepted value [7] of the pion life time, $\tau = 26$ ns, and a stopped pion fraction of $(11.4 \pm 0.2)\%$, which was in good agreement with the estimate from the Monte Carlo simulation.

Since the pions which stopped in the scintillator did not traverse the entire thickness, the effective target thickness for the 3.7 MeV data was slightly smaller, requiring a 1% correction to the cross section.

D. Pion fraction determination

For each run, the pion fraction was combined with the flux measurement described in the preceding section to determine the number of pions incident on the target. Because of the time structure of the LAMPF beam and the varying momentum acceptances used in the pion channel, determination of the pion fraction required somewhat different techniques and analyses at each energy, although the procedures used for the lowest energies were essentially the same. Since the publication of Ref. [4], we have completely reanalyzed our beam composition data to ascertain the pion fraction; the new results are not significantly different from those used before. The methods used at each energy are presented in detail below. The pion fraction analyses results are summarized in Table I, which also indicates typical values for the in-

TABLE I. Pion beam characteristics for the experiments described in this work. Given are the mean energies at the center of the target; the ratio $\eta = p_{c.m.}c/m_\pi c^2$, where $p_{c.m.}$ is the pion center-of-mass momentum and m_π is the pion rest mass; the standard deviations of the energy distributions; typical values for the pion fraction obtained; the uncertainty in the pion fraction; and the pion flux.

T_π (MeV)	η	ΔT_π (MeV)	f_π	δf_π (%)	N_π (s^{-1})
3.7	0.215	1.1	0.49	6	4×10^5
5.0	0.251	0.8	0.49	5	4×10^5
9.6	0.350	0.4	0.49	3	4×10^5
15.2	0.443	0.3	0.66	3	1.4×10^6
20.5	0.518	0.5	0.69	3	9.0×10^5

cident pion flux at the energies used in this experiment.

Typical target scintillator pulse height spectra are shown in Figs. 3, 4, and 5 for each of the cases described below. A Monte Carlo modeling program was used to estimate the pulse height distributions for the scintillators in the beam. The relative locations of the target scintillator pulse height peaks were well reproduced using this model, giving us confidence in the beam energy estimates noted above. However, this model did not reproduce the observed pulse height widths.

The widths of the peaks are due to the variation in

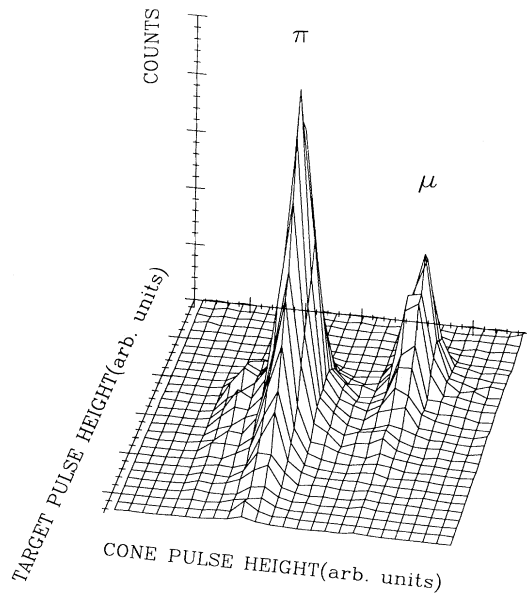


FIG. 3. Typical pulse height correlation for the deuterated scintillator target vs the downstream total absorption counter for the 20.5 MeV data runs. The downstream counter was identical to one of the $E - \Delta E$ telescope "cone" counters. Peaks resulting from pions and muons are indicated.

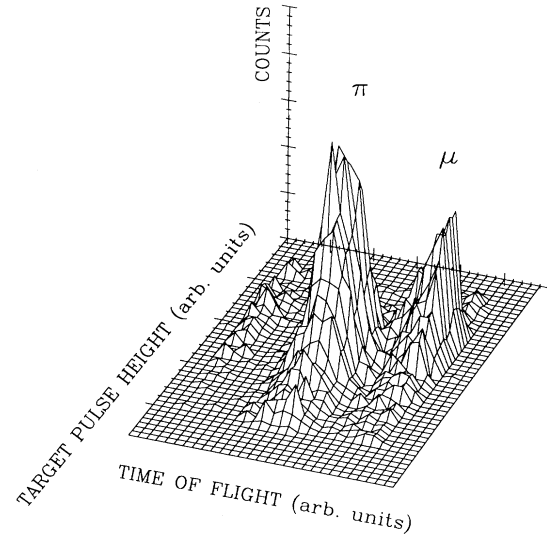


FIG. 4. Typical correlation histogram between target scintillator pulse height and time of flight, as described in the text, for the 15.2 MeV data runs. The peaks corresponding to pion and muon events are indicated.

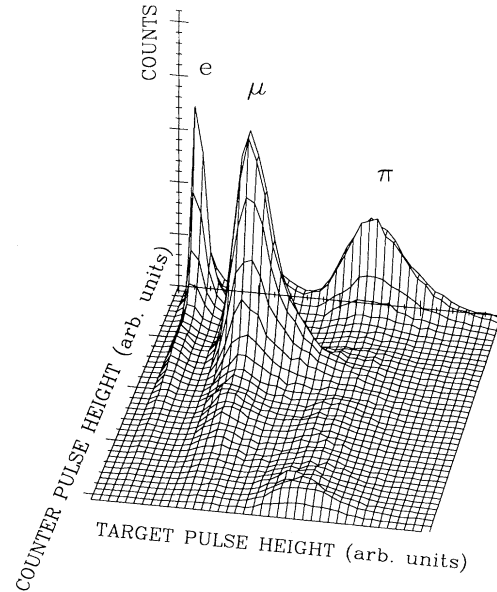


FIG. 5. Typical correlation histogram between target scintillator pulse height and downstream counter pulse height for the 5.0 MeV data runs. The positron, muon, and pion events are indicated. The pion events appear at a peak at the low end of the downstream counter pulse height spectrum and as a very broad peak at high pulse heights, which in this plot is cut off by an upper limit on the plot range. Typical 3.7 and 9.6 MeV histograms are similar.

light collection over the area of the target, the incident beam momentum spread, and pileup at high counting rates. With respect to this last contribution, a significant narrowing of the pulse height peaks was observed at each energy as the momentum spread of the channel was lowered in steps to 0.1%, primarily due to the reduction in counting rate. However, no appreciable change in beam composition was observed during variation of the momentum slit settings, although it was necessary to increase the estimated uncertainty for the determined pion fraction as the channel momentum acceptance was increased.

20.5 MeV data: At this energy, the pion fraction was determined by continuously sampling throughout the data taking runs the pulse height of the target scintillator and a downstream total absorption counter identical to one of the proton detector "cone" counters described below; a typical two-dimensional spectrum is shown in Fig. 3. Analysis of these spectra, including corrections for a tail on the large pulse height side of the pion peak, gave values for the pion fraction within each data run with relative uncertainties typically estimated to be less than $\pm 3\%$.

15.2 MeV data: The pion fraction for these runs was determined using pulse height information from the target scintillator correlated with the time difference between the accelerator 201.25 MHz accelerator RF master clock signal and the discriminator signal from the target scintillator. This technique takes advantage of the isochronous design of the LEP channel, but is practical only when the times of flight from the production target to the target scintillator for the different components of the beam are not multiples of the accelerator RF clock period of 5 ns, and when the momentum spread of the particles does not compromise the timing separation. These conditions were met only for the 15.2 MeV beam. A typical two-dimensional spectrum is shown in Fig. 4.

Particle identification of the time-of-flight peaks was verified by temporarily reducing the momentum acceptance of the channel to 0.1% and correlating the pulse height from a downstream scintillator with the target scintillator pulse height. This procedure also furnished an initial estimate of the pion fraction and an independent check on the value obtained in the final procedure.

The final value for the pion fraction was conservatively estimated by making two cuts on the time-of-flight spectrum for each run: one which clearly excluded enough pions to underestimate the pion fraction, and another which clearly included enough muons to overestimate the fraction. All counts which overflowed the range of the analog-to-digital converter (ADC) for the target scintillator pulse height were assigned as pions. Because of the sharpness of the pion peak, this generally required movement of the box cut by only one bin in the appropriate direction. The average of these two values was used as the estimate of the pion fraction, with half the difference as the uncertainty. The relative uncertainty in the pion fraction determination using this method was estimated to be $\pm 3\%$.

3.7, 5.0, and 9.6 MeV data: For these data, the pion fraction was determined by continuously correlat-

ing throughout the data taking runs the pulse height in the target scintillator with that obtained from a thin scintillator located 20.3 cm downstream. A typical spectrum is shown in Fig. 5 for the 5 MeV data. In that figure, it is seen that some of the pions appear at the low pulse height end of the downstream counter spectrum. These events correspond to pions that either did not reach the downstream counter at all or reached it with very low energy. The remaining pion events in the spectrum were distributed over a large range of pulse heights in the downstream counter, with approximately 30% being off scale. At 3.7 MeV, enough pions stopped in the downstream counter, as noted above, to necessitate a correction for effective target thickness. The analysis techniques, similar to those used for the 20.5 MeV spectra, yielded pion fraction estimates with relative uncertainties of the order of $\pm(3-6)\%$.

E. Reaction proton detection

Three pairs of plastic scintillator telescopes were used to detect the protons resulting from pion absorption in the deuterium target. These telescopes are the same as those described in Ref. [5], and their properties and operation are well understood. Each pair consisted of a "cone" telescope and a "wedge" telescope. The "cone" telescope was a thin scintillator disk followed by a thick truncated cone of plastic scintillator (Nuclear Enterprises NE-102). Although not exactly identical, the cones all were approximately 12.7 cm long, with end diameters of approximately 1.9 and 7.5 cm. These cone counters are deep enough to stop the reaction product protons, but require a correction for nuclear interactions. The large end of each cone was coupled directly to the cathode of a 8 cm photomultiplier tube. The thin scintillator disk, called a ΔE counter, was about 1.9 cm in diameter and 0.3 cm in thickness. It was mounted against the front of the cone, and coupled by a plastic light guide to a photomultiplier tube.

The complementary telescope of each pair was a wedge-shaped plastic scintillator approximately 8.9 cm wide \times 12.7 cm high \times 12.7 cm thick, and a 7.6×12.7 cm² \times 0.5 cm thick scintillator mounted against the front of the wedge. Each of the wedge scintillators was coupled directly to the cathode of a 13 cm photomultiplier tube, and the ΔE scintillator was coupled by a light guide to a 5 cm tube. The general placement of the wedge and cone counters is indicated in Fig. 1.

The counters were positioned approximately 30 cm from the deuterated scintillator target on a table inscribed with angle radials. The counters were placed so that the solid angle for each telescope pair was determined entirely by the ΔE counter on the "cone" detector. Target-to- ΔE counter distances and ΔE counter dimensions were measured following the experiment in order to determine their respective solid angles; these solid angles, as determined with a Monte Carlo program to model the finite size of beam spot and detectors, were 9.95 ± 0.03 , 9.20 ± 0.03 , and 9.17 ± 0.03 msr.

The protons from absorption on deuterium were well separated from those from absorption on carbon within

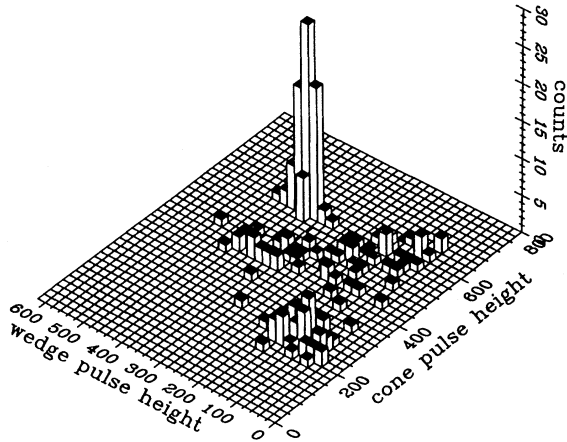


FIG. 6. Typical reaction product proton energy correlation for the members of a proton detector telescope pair. The prominent peak arises from pion absorption on deuteron. That peak is seen to be separated well from the lower energy carbon absorption events.

the target, as can be seen in Fig. 6. The spectra are characterized by a strong reaction peak, with tails from protons undergoing nuclear interactions. Cuts were made on these spectra at the edge of the carbon band, and corrections for the protons missed by such a cut were made based on the energy at which the cut was made. The energy-dependent corrections for nuclear interactions of the protons within these particular counters had been empirically measured previously [8]. Those corrections, ranging from 4% to 23% with absolute uncertainties of less than 1%, were applied to the data for the present experiment. Two or more different configurations of the proton detectors were used to provide checks on systematic errors or to increase angular coverage.

III. RESULTS

The center-of-mass differential cross sections for each counter are given by

$$\frac{d\sigma}{d\Omega} = \frac{N_p}{N_\pi n J \Delta\Omega},$$

where N_p is the number of proton reaction pairs corrected for interactions, N_π is the pion flux through the target, n is the deuteron areal density of the target, J is the laboratory-to-center-of-mass frame Jacobian, and $\Delta\Omega$ is the ΔE counter solid angle. For this work, all data and estimates have been reexamined as noted above. Only in one instance, an incorrectly recorded cross section at one angle of the 15.2 MeV data set, are the cross sections determined here different from the analysis previously published in Ref. [4].

The center-of-mass differential cross sections determined in this experiment are given in Table II and displayed in Fig. 7. Even at the lowest energy for which measurements were made here, the cross sections remain clearly anisotropic. As reported in Ref. [4], these dif-

ferential cross sections were fit using the form $d\sigma/d\Omega = \alpha_0 P_0(\cos\theta_{c.m.}) + \alpha_2 P_2(\cos\theta_{c.m.})$, where $P_n(\cos\theta)$ are the Legendre polynomials of order n . The parameters obtained are given in Table III with statistical errors only.

Using this form to fit the angular distributions, the total cross section is equal to $2\pi\alpha_0$. The total cross sections thus determined were found to be 4.0 ± 0.5 , 4.4 ± 0.2 , 4.2 ± 0.2 , 4.15 ± 0.18 , and 4.8 ± 0.3 mb for incident pion energies of 3.7, 5.0, 9.6, 15.2, and 20.5 MeV, where the uncertainties include both the statistical and the absolute normalization uncertainties. Absolute normalization uncertainties are attributable to uncertainties in the measurements of the beam pion fraction at each energy and in the areal density of the target as described above.

The results obtained here have been compared with other experimental and theoretical work in Ref. [4]. We note here again that the measurements are in excellent agreement with Hutcheon *et al.* and with Ref. [5], and confirm that significant p -wave strength exists even at the lowest energy measured here. As noted in both Refs. [3] and [4], there is no indication of any breaking of charge independence in the data obtained here and for the $n\pi \rightarrow d\pi^0$ reaction.

For comparison with existing theoretical predictions for the reaction, we have chosen to compare the data reported here with the Faddeev-like treatment of Blankleider and Afnan (BA) [9] and the perturbation theory approach of Vogelzang, Bakker, and Boersma (VBB) [10]. The BA work used a set of equations which explicitly coupled the NN and πd reaction channels, permit-

TABLE II. Center-of-mass differential cross sections for $\pi^+ + d \rightarrow p + p$ measured in this study. Statistical uncertainties are given for the cross sections in parentheses.

T_π (MeV)	$\theta_{c.m.}$ (deg)	$d\sigma/d\Omega$ (mb/sr)
3.7	25.0	0.78(7)
	62.2	0.60(9)
5.	25.2	0.87(4)
	37.7	0.82(4)
	62.5	0.65(4)
9.6	25.6	0.86(4)
	38.4	0.77(7)
	51.0	0.77(8)
	63.4	0.60(4)
15.2	26.0	1.02(3)
	38.9	0.84(4)
	51.7	0.76(6)
	64.3	0.54(2)
20.5	70.5	0.54(10)
	26.3	1.14(5)
	39.4	0.93(5)
	58.6	0.73(4)

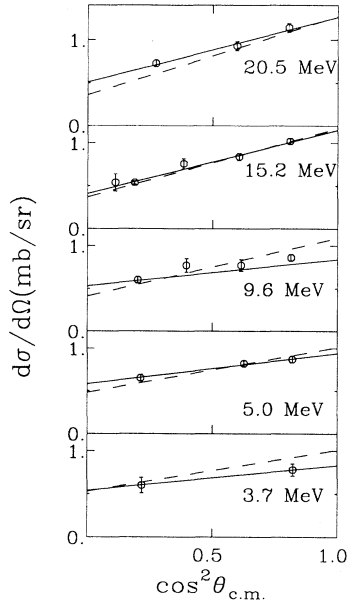


FIG. 7. Differential cross sections measured in this experiment. Also shown are the results of the Legendre polynomial fits described in the text (solid line) and the results from the parametrization from Ref. [12] (dashed line).

ting a “unified” set of predictions for the $NN \rightarrow NN$, $NN \rightarrow \pi d$, and $\pi d \rightarrow \pi d$ reactions. This unified treatment provided an approach which respected unitarity in the three reaction channels studied. The BA results were in good agreement with the total and differential cross sections for $\pi d \rightarrow pp$ over the energy region from 40 to about 250 MeV, where the use of nonrelativistic kinematics resulted in overprediction of the observed cross sections.

In the VBB work, several different approaches were employed examining the importance of different treatments of the reaction mechanism, including the contributions arising from rescattering of pions moving forward and backward in time. The best agreement with the existing data over the entire energy range from about 3 to

TABLE III. Parametrization of differential cross sections measured in this experiment as described in the text. Except for the total cross section, uncertainties listed are statistical only. The uncertainties for the total cross section include systematic errors.

T_π (MeV)	α_0 (mb/sr)	α_2 (mb/sr)	σ_{tot} (mb)
3.7	0.63(7)	0.19(12)	4.0(5)
5.0	0.70(3)	0.24(6)	4.4(2)
9.6	0.67(3)	0.28(6)	4.2(2)
15.2	0.66(2)	0.50(3)	4.15(18)
20.5	0.76(4)	0.51(8)	4.8(3)

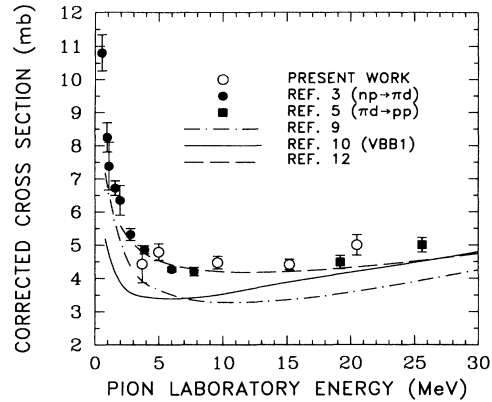


FIG. 8. Coulomb-corrected total cross sections measured in this work and in Refs. [5] for the reaction $\pi^+ + d \rightarrow p + p$, and the results of Ref. [3] for the reaction $n + p \rightarrow d + \pi^0$, which require no Coulomb corrections. Also shown are predictions from Refs. [9, 10] and results from the parametrization of Ref. [12].

about 180 MeV was found for their “standard-1” calculation (VBB1). The results of the VBB study indicated that the complete pion propagator, including backward moving pions, was essential in achieving predictions in reasonable agreement with experiment.

There is significant disagreement between the BA and VBB theoretical predictions for the observed energy dependence of the total cross section in this region and the measurements reported here and in Refs. [2, 3]. This disagreement can be seen in Fig. 8, where the data have been corrected for Coulomb effects using the results of Reitan [11]. (The BA and VBB calculations did not include Coulomb effects, so no adjustments of the calculations are required to perform the comparison shown in Fig. 8.) Since the data for the reaction at energies below 20 MeV which existed at the time of both calculations possessed large uncertainties as noted above, the deficiencies in the calculations may lie principally in the treatment of the s -wave contributions, which are of much greater importance in the energy region studied here than at energies above 20 MeV.

The values for the total and differential cross sections using a recent parametrization [12] of the data below 1 GeV are indicated in Figs. 7 and 8 and are seen to be in good agreement with the data shown in those figures.

IV. CONCLUSION

Absolute total and differential cross sections have been measured for the reaction $\pi^+ + d \rightarrow p + p$ for energies below 21 MeV. The cross sections indicate the presence of p -wave strength down to the lowest energy measured, as was seen for the $n + p \rightarrow d + \pi^0$ measurements near threshold in Refs. [2, 3]. While in agreement with a recent parametrization of the total and differential cross section energy dependence, the data found here and in

Refs. [2, 3, 5] are in disagreement with the theoretical predictions in this energy region by Refs. [9, 10]. With the remarkably good agreement present for both the BA and VBB approaches at higher energies, a reexamination of models for the reaction, particularly their treatment of the *s*-wave contributions to the reaction mechanism, in light of the refined data set which now exists at lower energies would be both timely and useful.

ACKNOWLEDGMENTS

We gratefully acknowledge the support of the staff at LAMPF, particularly J. A. McGill, and of E. D. Loughran and D. G. Ott of the Los Alamos National Laboratory. This work was supported in part by the National Science Foundation and the U.S. Department of Energy.

-
- [1] C. M. Rose, *Phys. Rev.* **154**, 1305 (1967).
 - [2] D. A. Hutcheon, E. Korkmaz, G. A. Moss, R. Abegg, N. E. Davison, G. W. R. Edwards, L. G. Greeniaus, D. Mack, C. A. Miller, W. C. Olsen, I. J. van Heerden, and Ye Yanlin, *Phys. Rev. Lett.* **64**, 176 (1990).
 - [3] D. A. Hutcheon, E. Korkmaz, G. A. Moss, R. Abegg, N. E. Davison, G. W. R. Edwards, L. G. Greeniaus, D. Mack, C. A. Miller, W. C. Olsen, I. J. van Heerden, and Ye Yanlin, *Nucl. Phys.* **A535**, 618 (1991).
 - [4] B. G. Ritchie, R. C. Minehart, T. D. Averett, G. S. Blanchard, K. Giovanetti, B. M. Preedom, D. Rothenberger, L. C. Smith, and J. R. Tinsley, *Phys. Rev. Lett.* **66**, 568 (1991).
 - [5] B. G. Ritchie *et al.*, *Phys. Rev. C* **24**, 552 (1981).
 - [6] R. L. Burman *et al.*, *Nucl. Instrum. Methods.* **131**, 29 (1975).
 - [7] J. J. Hernandez *et al.*, *Phys. Lett. B* **239**, 1 (1990).
 - [8] B. M. Preedom, M. J. Saltmarsh, C. A. Ludemann, and J. Alster, *Nucl. Instrum. Methods.* **133**, 311 (1976).
 - [9] B. Blankleider and I. R. Afnan, *Phys. Rev. C* **24**, 1572 (1981).
 - [10] J. Vogelzang, B. L. G. Bakker, and H. J. Boersma, *Nucl. Phys.* **A452**, 644 (1986).
 - [11] A. Reitan, *Nucl. Phys.* **B11**, 170 (1969).
 - [12] B. G. Ritchie, *Phys. Rev. C* **44**, 533(1991).